in paraffin. Tissue samples from adult mice were decalcified in 20% EDTA for 2 weeks after fixation before being embedded in paraffin. Sections were stained with 0.1% Safranin O (orange stain) to evaluate cartilage matrices, and 0.03% fast green to evaluate morphologic features, as previously described (13). In situ hybridization was performed using ^{35}S-labeled riboprobes according to the standard protocol as described previously (7). Hybridizations were performed at 55°C.

Autoradiography and Hoechst 33528 staining were performed as previously described (7). For staining with LacZ, tails from Runx2-heterozygote mice were fixed in 0.2% paraformaldehyde at room temperature for 30 minutes, and then stained overnight in X-Gal solution as previously described (7). The following day, samples were decalcified and processed for histologic examination.

Immunohistochemistry was performed according to a standard protocol (7). Anti-Runx1 antibody (14) and anti–α1(X) collagen antibody were purchased from Santa Cruz Biotechnology (Santa Cruz, CA) and Cosmo Bio (Tokyo, Japan), respectively. The anti-Runx2 and anti-Runx3 antibodies have been described previously (7,15). Six mice per group were analyzed, and identical phenotypes were observed.

Disc compression of mouse vertebrae and analysis of IVDs in human patients. The vertebrae of 8-week-old female WT mice were compressed as previously described, with minor modifications (16). Briefly, the ninth and tenth caudal vertebrae were percutaneously punctured by 0.4-mm stainless steel pins and transfixed. Subsequently, the pins were instrumented using elastic springs. After 1–4 weeks, the mice were dissected and the vertebrae were examined histologically. Four mice per group were analyzed, and identical phenotypes were observed.

The study protocol involving human patients was approved by a local ethics committee. Patients with IVD degeneration were classified according to an established grading system (17). Patients with moderate disc degeneration (grade 3 to grade 4) (17) gave written informed consent for the collection of their RNA from the degenerated disc at the time of surgery. As a control, we used patients with spinal cord injury whose IVDs had no detectable damage. RNA was extracted from the IVD samples and reverse-transcribed. Expression of *Runx*2 was quantitatively analyzed by real-time quantitative PCR.

RESULTS

Comparison of *Runx*1, *Runx*2, and *Runx*3 expression during mouse skeletal development. As an initial way to assess the respective contribution of each of the 3 *Runx* genes to chondrocyte differentiation, we used in situ hybridization to study their pattern of expression in the developing mouse skeletons between embryonic day 12.5 and birth. The identity of the cells expressing each *Runx* gene was determined on adjacent tissue sections using different probes, as follows: α1(I) collagen as a marker of fibroblasts and osteoblasts, α1(II) collagen as a marker of proliferating and prehypertrophic chondrocytes, α1(X) collagen as a marker of hypertrophic chondrocytes, and Indian hedgehog as a marker of prehypertrophic chondrocytes (18). This analysis was performed in vertebrae and in long bones, since chondrocyte differentiation has been extensively studied on a molecular level in both of these sites.

At embryonic day 12.5, *Runx*2 was expressed in mesenchymal cells of the perichondrium of the vertebrae (Figure 1A, arrow), but not in cells located in the vertebral body. Expression of *Runx*2 was also observed in cells of Meckel's cartilage (results not shown). These results indicate that at this stage of development, *Runx*2 was expressed in prechondrogenic cells. *Runx*1, at embryonic day 12.5, was expressed in α1(II) collagen–positive cells of the perichondrium of the vertebrae (Figure 1A, arrow), as well as in the dorsal root ganglia. In contrast, *Runx*3 expression was observed in chondrocytes in vertebral bodies (Figure 1A, arrowhead).

The chondrocytes of vertebral bodies strongly expressed Indian hedgehog (Figure 1A), suggesting that these chondrocytes were destined to become prehypertrophic. At embryonic day 14.5 and at later stages of embryonic development, *Runx*1 expression in chondrocytes was low, whereas *Runx*2 was expressed in the prehypertrophic and hypertrophic chondrocytes, and *Runx*3 was expressed in the prehypertrophic chondrocytes (Figures 1B and C and results not shown).

Results of these analyses demonstrate that all *Runx* genes are expressed at some developmental point in cells of the chondrocyte lineage. However, they have a complex and dynamic pattern of expression during chondrogenesis. These observations led us to examine the role of each of the Runx proteins in chondrogenesis.

Generation of transgenic mice expressing *Runx*1 or *Runx*3 in nonhypertrophic chondrocytes throughout development. We have previously shown that constitutive expression of *Runx*2 in nonhypertrophic chondrocytes resulted in premature differentiation of hypertrophic chondrocytes in long bones and in ectopic differentiation of hypertrophic chondrocytes in chondrocostal cartilage (7). The high structural similarity of the Runx proteins (Figure 2A) and their overlapping expression in chondrocytes (Figure 1) prompted us to examine the roles of Runx1 and Runx3 in chondrocyte differentiation. To accomplish this, we generated transgenic mice expressing either *Runx*1 or *Runx*3 cDNA under the control of a 3-kb–long fragment of the mouse α1(II) collagen promoter and its 3-kb–long chondrocyte-specific enhancer (19) (Figure 2A); these transgenic mice were termed α1(II)-*Runx*1 and α1(II)-*Runx*3 mice, respectively.

The expression of the transgene in α1(II)-*Runx*1 or α1(II)-*Runx*3 mice was confirmed by real-time quantitative PCR using RNA extracted from transgenic embryos. Transgene expression was restricted to the cartilage, and the expression level was

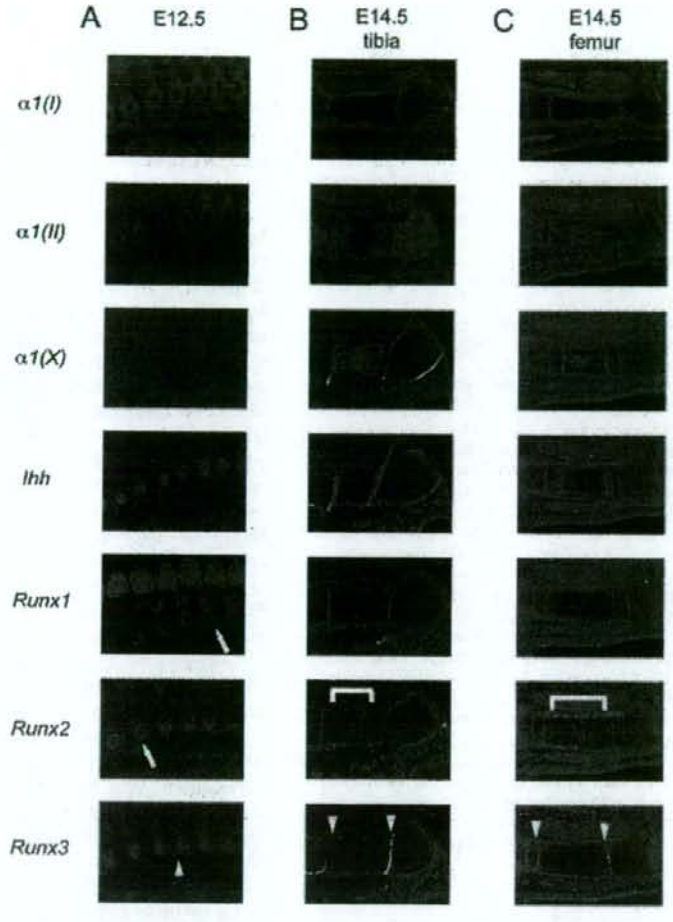

Figure 1. Analysis of *Runx* gene expression by in situ hybridization in the mouse vertebrae at embryonic day (E) 12.5 (**A**) and in the tibia (**B**) and femur (**C**) at embryonic day 14.5. Adjacent sections of wild-type mouse embryos were hybridized with the indicated probes. Note the expression of *Runx*1 and *Runx*2 in condensations of mesenchymal cells (**arrow**) (**A**), the broad expression of *Runx*2 in nonhypertrophic chondrocytes (**bracket**) (**B** and **C**), and the restricted expression of *Runx*3 in prehypertrophic chondrocytes (**arrowheads**) (**A–C**). Ihh = Indian hedgehog.

comparable with that of the α1(II)-*Runx*2 transgene (Figure 2B). We obtained 2 lines for the α1(II)-*Runx*1 mice, and both lines were born at the expected Mendelian ratio and showed no overt abnormalities at birth (results not shown). In contrast, the α1(II)-*Runx*3 mice never survived until birth, and therefore analysis of these mice was performed only on skeletal preparations from transgenic embryos.

Ectopic hypertrophic chondrocyte differentiation and endochondral ossification in α1(II)-*Runx*3 embryos, but not in α1(II)-*Runx*1 mice. In order to study skeletal cell differentiation, we first used Alcian blue/alizarin red to stain skeletal preparations (20). Alcian blue stains were used to reveal demineralization of cartilaginous matrices, while alizarin red stains showed mineralization of cartilaginous and bony matrices.

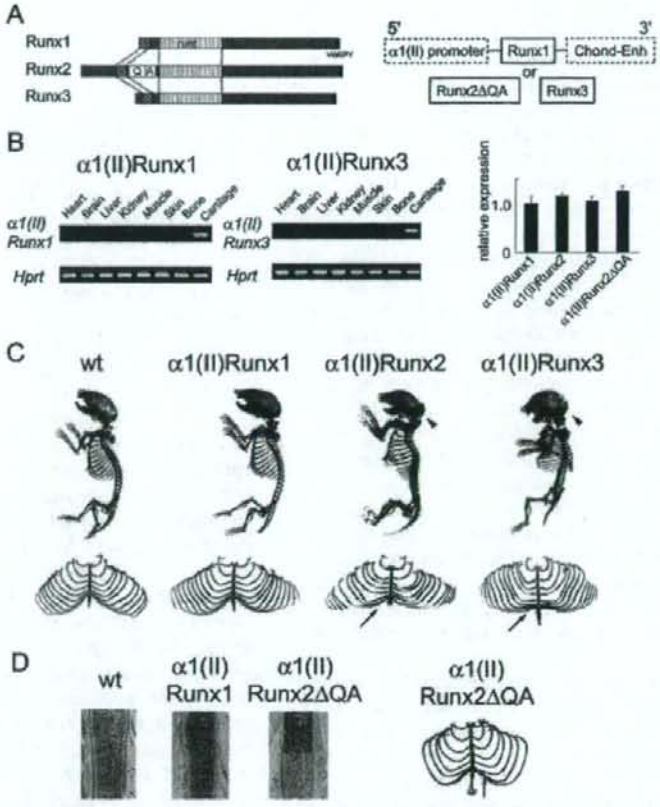

Figure 2. **A** and **B**, Generation of α1(II)-*Runx*–transgenic mice. **A**, Left, Comparison of the structures of the Runx proteins, which share a highly homologous runt domain. Right, Schematic representation of the construct used. Transgenic mice containing *Runx*1, *Runx*2ΔQA (lacking the QA domain of Runx2), or *Runx*3 cDNA were generated under the control of a chondrocyte-specific α1(II) collagen promoter/enhancer (Chond-Enh) cassette. **B**, Left, Cartilage-specific expression of each transgene in the α1(II)-*Runx*1 and α1(II)-*Runx*3 mice. Hypoxanthine guanine phosphoribosyltransferase (*Hprt*) amplification was used as an internal control. Right, Quantitative analysis of transgene expression by real-time polymerase chain reaction. Bars show the mean and SD relative expression. **C** and **D**, Ectopic and accelerated mineralization of cartilage in α1(II)-*Runx* mice as compared with wild-type (WT) mice. **C**, Alcian blue/alizarin red staining of skeletal preparations at birth, revealing ectopically mineralized areas in chondrocostal cartilage (**arrow**) and accelerated chondrocranium mineralization (**arrowhead**) in α1(II)-*Runx*2 and α1(II)-*Runx*3 mice, both of which were lacking in WT and α1(II)-*Runx*1 mice. **D**, Left, Histologic analysis of α1(II)-*Runx* mice by Safranin O staining of sections through chondrocostal cartilage, revealing the displacement of cartilage with bone marrow cavity in α1(II)-*Runx*2ΔQA mice, but not in α1(II)-*Runx*1 mice. Right, Alcian blue/alizarin red staining of skeletal preparations from α1(II)-*Runx*2ΔQA mice at 1 month of age, revealing the restricted appearance of ectopic mineralization (**arrow**).

The most striking phenotypic abnormality in the α1(II)-*Runx*3 embryos prebirth was ectopic calcification of the rib cage. In WT embryos, the frontal part of the rib cage, also called chondrocostal cartilage, never mineralized during development or throughout life, since chondrocyte hypertrophy does not occur in this cartilage. As a result, chondrocostal cartilage always stained blue in WT embryos (Figure 2C) and in adult mice. In contrast, the chondrocostal cartilage of α1(II)-*Runx*3 embryos stained red, indicating the existence of ectopic mineralization (Figure 2C, arrow). This phenotypic abnormality was identical to that observed in the α1(II)-*Runx*2 mice (Figure 2C, arrow), and reflected the presence of hypertrophic chondrocytes (7). However, the onset and extent of this phenotype was earlier and more severe in the α1(II)-*Runx*3 mice.

In contrast, neither the chondrocostal cartilage nor the chondrocranium ever stained red in α1(II)-

*Runx*1 mice at birth (Figure 2C). Consistent with the absence of ectopic red staining in the *Runx*1 mice at birth, histologic examination of the chondrocostal cartilage of these mutant mice failed to reveal any evidence of ectopic chondrocyte hypertrophy (Figure 2D). Therefore, these results indicate that the different Runx proteins each possess a distinct potential to induce ectopic chondrocyte hypertrophy, in which Runx2 and Runx3 can induce ectopic chondrocyte hypertrophy, whereas Runx1 cannot.

In addition to the ectopic endochondral mineralization observed, there was also premature endochondral ossification in other areas of the skeleton, such as the chondrocranium, in α1(II)-*Runx*3 and α1(II)-*Runx*2 mice (Figure 2C, arrowheads). In the α1(II)-*Runx*3 mice at birth, the chondrocranium stained red and the head circumferences were smaller, whereas the chondrocranium of the WT mice stained blue. In contrast, in the α1(II)-*Runx*1 mice at birth, the chondrocranium was never observed to be mineralized (Figure 2C).

The histologic findings in the growth plate of α1(II)-*Runx*1 mice were indistinguishable from those in the growth plate of WT mice at all stages analyzed, in the embryo and after birth (results not shown). Thus, Runx3 and Runx2, but not Runx1, possess the ability to accelerate the normal program of chondrocyte differentiation.

Potentiation of the ability of Runx2 to induce hypertrophic chondrocyte differentiation via the Runx2 QA domain. A unique glutamine–alanine (QA) motif is present in the amino-terminus of the runt domain of Runx2, but not in Runx1 or Runx3 (Figure 2A). In order to address the role of the QA domain in chondrocyte differentiation, we generated transgenic mice by inducing expression of a mutant form of Runx2 (11) in which the QA domain was lacking (comprising the α1(II)-*Runx*2ΔQA group of mice) (Figure 2A). Surprisingly, these mice also developed ectopic mineralization, similar to that observed in the α1(II)-*Runx*2 mice, at 1 month of age (Figure 2D), indicating that the chondrocyte differentiation ability of Runx2 does not lie solely in this domain.

Histologically, the mineralized cartilage in α1(II)-*Runx*2ΔQA mice was ectopically invaded by the bone marrow cavity (Figure 2D). However, whereas most of the male α1(II)-*Runx*2 mice died perinatally (13 of 14 transgenic mice) due to ectopic mineralization of the rib cage, none of the α1(II)-*Runx*2ΔQA mice (0 of 14 transgenic mice) died before the age of 1 month. Moreover, the extent of ectopic mineralization was significantly less severe in α1(II)-*Runx*2ΔQA mice than in α1(II)-*Runx*2 mice. These results suggest that, although the QA domain of Runx2 is not essential, it does potentiate the ability of Runx2 to differentiate chondrocytes.

Evidence of IVD degeneration in α1(II)-*Runx*1 and α1(II)-*Runx*2 mice. Since α1(II)-*Runx*1 mice had a normal lifespan, we investigated whether Runx1 plays other roles in the chondrocyte later in life. Surprisingly, starting at 3 months of age, 52% of the α1(II)-*Runx*1 mice (12 of 23 mice) developed kyphosis and scoliosis ($P < 0.01$ versus WT mice); by 6 months of age, all of the male and female α1(II)-*Runx*1 mice exhibited these features. In contrast, no such abnormalities were observed in WT mice. Radiographic evaluation revealed deformities of the vertebrae and IVD degeneration in the α1(II)-*Runx*1 mice (Figure 3A). This phenotype led us to analyze the integrity of the IVDs in these transgenic mice.

Histologic analysis showed that the IVDs of the WT mice were composed of 3 different tissue types: cartilaginous endplate of adjacent vertebrae bodies, outer annulus fibrosus, which is composed of dense, spatially oriented α1(I) collagen fibrils, and inner nucleus pulposus, a notochord remnant (21) that is mostly (80–90%) composed of water (Figure 3B). In the α1(II)-*Runx*1 mice, there was ectopic accumulation of extracellular matrix in the IVDs at ~3 months of age (Figure 3B), although the mice had not shown any abnormalities at 1 month of age (results not shown). In addition, Schmorl's node, an abnormal herniation of fibrocartilaginous tissue through the endplate and, thus, a hallmark of endplate degeneration, was also observed in α1(II)-*Runx*1 mice at 3 months of age (Figure 3D, arrow). At 6 months of age, the organized structure of the annulus fibrosus was lost, and the inner nucleus was totally replaced by extracellular matrices and had become dehydrated (Figure 3B, arrow). Also, clusters of hypertrophic chondrocytes stained positive by immunohistochemistry for α1(X) collagen (Figure 3C, arrow), although this had never been observed in the WT mice.

To determine whether this was a specific feature of Runx1 or whether other Runx proteins could also affect the integrity of the IVD later in life, we analyzed adult α1(II)-*Runx*2 mice. Similar to that observed in the α1(II)-*Runx*1 mice, the α1(II)-*Runx*2 mice that survived perinatally also developed IVD degeneration by 3 months of age (Figures 3A and B, arrow). Histologically, there was ectopic differentiation of hypertrophic chondrocytes in the IVDs of the α1(II)-*Runx*2 mice (Figure 3C, arrow), as was observed in the α1(II)-*Runx*1 mice. Collectively, these results indicate that when the Runx proteins are overexpressed, they can affect IVD integrity.

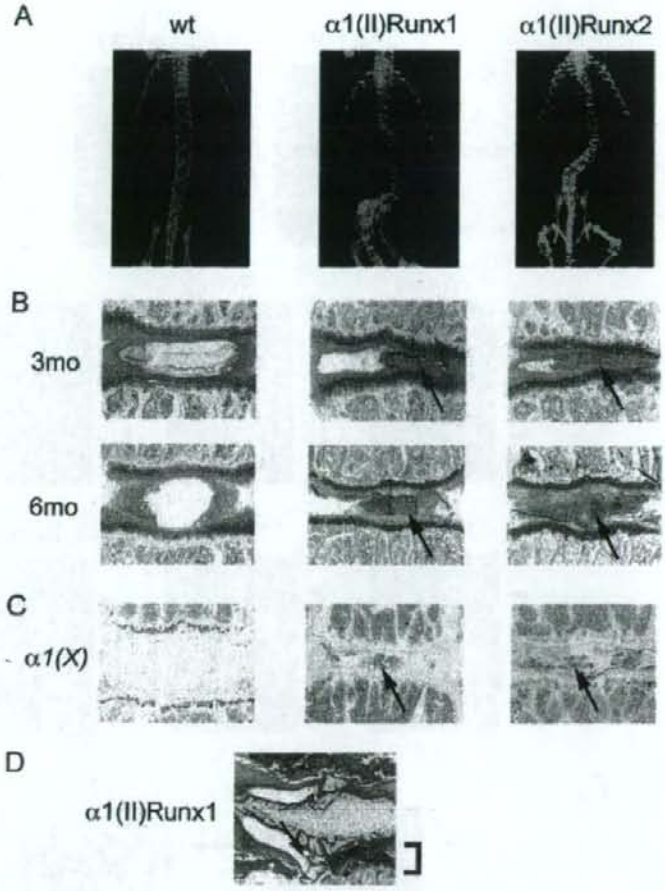

Figure 3. Intervertebral disc (IVD) degeneration in α1(II)-*Runx*1 and α1(II)-*Runx*2 mice. **A,** Radiographic analysis of the vertebrae at 3 months revealed marked scoliosis in the IVDs of α1(II)-*Runx* mice as compared with wild-type (WT) mice. **B–D,** Coronally cut sections of the IVDs, along with adjacent vertebral bodies, were assessed histologically by Safranin O staining (**B** and **D**), and by immunohistochemistry (**C**), which showed ectopic α1(X) collagen expression. Note the progressive degeneration of the IVDs and displacement by extracellular matrix in the α1(II)-*Runx*1 and α1(II)-*Runx*2 mice (**arrow**) (**B** and **C**), and the protrusion of the IVD (**arrow**) through the endplate into the columnar growth plate (**bracket**) in α1(II)-*Runx*1 mice (**D**).

Induction of *Runx* gene expression in the cartilaginous endplate following weight loading. The fact that there were phenotypic abnormalities in adult α1(II)-*Runx*1 and α1(II)-*Runx*2 mice suggested that the Runx proteins may have an as yet unappreciated function in the IVD. To address this question, we first analyzed the expression of *Runx* genes in IVDs during embryonic development. At embryonic day 16.5, all of the *Runx* genes were expressed in specific regions of the vertebral body and/or the IVD (Figure 4A). *Runx*1 was mainly expressed in the primary ossification center. *Runx*2 was also expressed in the ossification center, in chondrocytes and cells surrounding the prospective IVD. *Runx*3 was specifically expressed in prehypertrophic chondrocytes.

We also analyzed the expression of each Runx protein by immunohistochemistry, which revealed identical patterns of expression between the 3 proteins

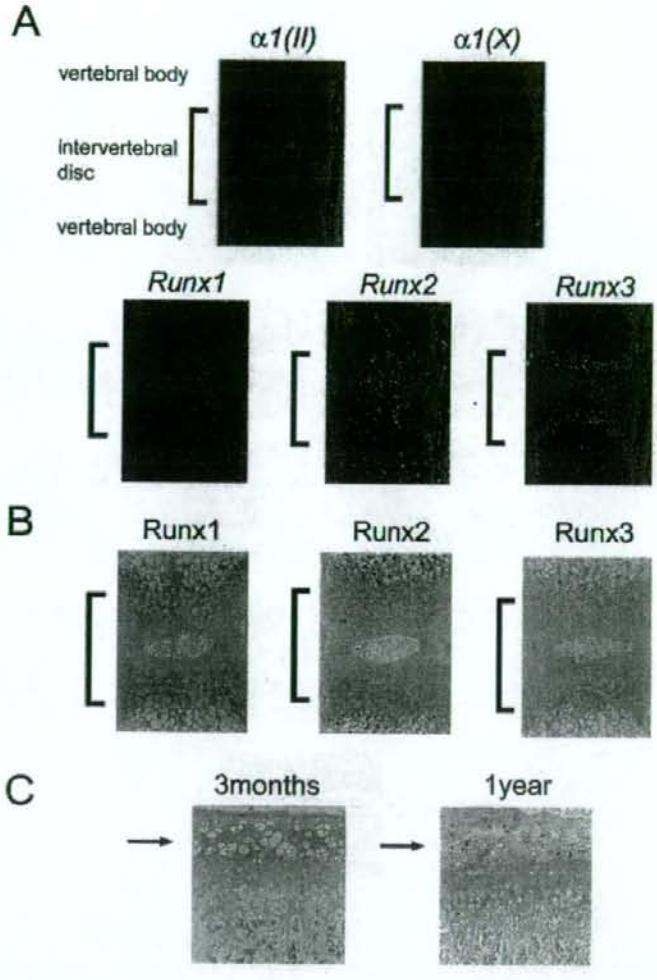

Figure 4. Expression of *Runx*2 in intervertebral discs (IVDs). Adjacent sections of wild-type mouse embryos at embronic day 16.5 were assessed by in situ hybridization using the indicated probes **(A)**, and by immunohistochemical analysis **(B** and **C)**. Note the expression of *Runx*2 in the prospective IVD **(bracket)** (**A** and **B**). Immunohistochemical analysis of the IVDs after birth revealed that *Runx*2 was not expressed in the wild-type mice at 3 months of age, but was expressed at 1 year **(arrow)** (**C**).

(Figure 4B). These analyses showed that Runx2 was the only member of the family that was physiologically expressed in the prospective IVD.

We next analyzed *Runx*2 expression in the IVDs of WT mice after birth. Whereas the expression of *Runx*2 in the IVDs was close to background values at 1 month and 3 months of age (results not shown and Figure 4C), it had increased in the endplate of the IVDs of WT mice at 1 year (Figure 4C, arrow).

Since the overexpression of *Runx*1 or *Runx*2 led to degeneration of the IVD, and Runx2 protein was detected in the IVD, we tested whether *Runx*1 or *Runx*2 induces IVD degradation in pathologic conditions. To test this possibility, we analyzed the biomechanical func-

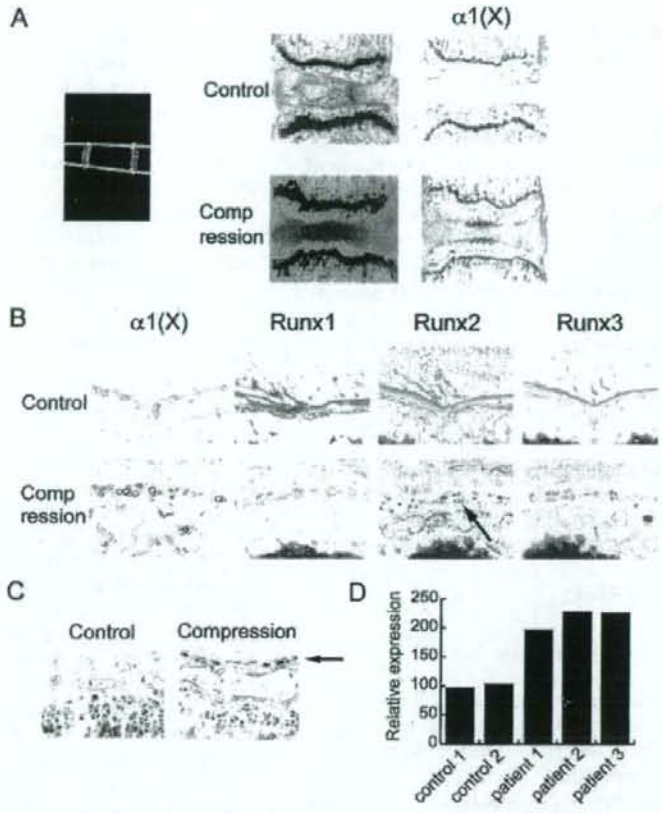

Figure 5. Evaluation of intervertebral disc (IVD) degeneration in mice and humans. **A,** Induction of *Runx*2 expression by mechanical compression in a mouse model of IVD degeneration. Caudal vertebrae from 2-month-old wild-type mice were compressed by an elastic spring, and then assessed by radiography (left), histology (middle), and immunohistochemistry (with Safranin O staining) (right). The compressed IVDs showed degeneration and ectopic α1(X) collagen expression (right). **B,** Immunohistochemical analysis of the expression of Runx proteins in adjacent sections of the compressed vertebrae. Note the specific induction of Runx2 in the endplate of the compressed vertebrae **(arrow)**, with coexpression of α1(X) collagen. **C,** Induction of *Runx*2 mRNA expression by compression. Vertebrae from *Runx*2$^{+/-}$ mice were compressed and analyzed by LacZ staining. Note the specific induction of *Runx*2 mRNA in the endplate **(arrow)**. **D,** Up-regulation of *Runx*2 in human patients with IVD degeneration. Quantitative polymerase chain reaction showed that *Runx*2 expression was significantly up-regulated in patients with IVD degeneration compared with unaffected control subjects.

tion of the IVDs of WT mice in a model of mechanical stress–induced compression, the most frequent cause of IVD degeneration. For this test, we transfixed the vertebral body with steel wire and instrumenting elastics for 4 weeks (Figure 5A), and compared Runx protein accumulation before and after compression.

After compression of the IVDs, typical disc degeneration was observed, in the form of a damaged endplate and massive induction of cells positive for type X collagen, which indicated the appearance of hypertrophic chondrocytes (Figure 5A). *Runx*1 expression was undetectable before and after compression (Figure 5B), suggesting that *Runx*1 does not contribute to IVD degeneration under these conditions. *Runx*3 expression was observed after compression, albeit at a very low level (Figure 5B). In sharp contrast, there was strong induction of Runx2 protein expression in the endplate after compression (Figure 5B, arrow). Moreover, cells expressing Runx2 also expressed α1(X) collagen, indicative of the appearance of hypertrophic chondrocytes (Figure 5B).

We took advantage of the LacZ allele that was inserted in the *Runx*2 locus in *Runx*2$^{+/-}$ mice. *Runx*2 messenger RNA (mRNA) expression can be monitored by LacZ staining in these mice. Before compression, we were able to observe *Runx*2 mRNA expression in osteoblasts on bone trabeculae and growth-plate chondrocytes, but not in the endplate, demonstrating that expression of *Runx*2 was minimal. Surprisingly, after compression, numerous LacZ-positive cells were observed in the cartilaginous endplate (Figure 5C), thus demonstrating that compression induced *Runx*2 expression.

Up-regulation of Runx2 in human IVD degeneration. Finally, to determine if the induction of Runx2 is also involved in the development of IVD degeneration in humans, we analyzed *Runx*2 mRNA expression in patients with moderate disc degeneration. We collected RNA from the affected IVDs of these patients, and compared the RNA levels with those in intact IVDs as a control. Similar to that observed in the mouse model, expression of *Runx*2 mRNA was up-regulated in all patients with IVD degeneration examined (Figure 5D). Taken together, these results clearly demonstrate that in both mice and humans, IVD degeneration is accompanied by induction of Runx2.

DISCUSSION

On the basis of previous findings showing that Runx2 is an important regulator of chondrocyte hypertrophy, we examined the role of other Runx family members, Runx1 and Runx3, in chondrocytes, particularly in chondrocyte differentiation in vivo, and compared these results with those obtained for Runx2. Overexpression of *Runx*1, *Runx*2, or *Runx*3 in nonhypertrophic chondrocytes led to skeletal abnormalities, indicating that the expression of these genes at precise times during skeletal development and chondrocyte differentiation is important, and that each gene must have a distinct role in the differentiation of chondrocytes.

In addition to the ectopic mineralization observed, overexpression of *Runx*1 or *Runx*2 led to IVD degeneration. We showed that Runx2 is the only family member normally expressed in the IVD, and that Runx2 expression, along with chondrocyte hypertrophy, were induced in a mouse model of IVD degeneration. Finally, we demonstrated that in human patients with IVD degeneration, Runx2 expression was significantly up-regulated, thus suggesting that Runx2 contributes to the pathogenesis of IVD degeneration through the induction of chondrocyte hypertrophy.

In the present study, *Runx*1 expression in WT mice was restricted mostly to progenitor cells that were not yet committed to either the chondrocyte or the osteoblast lineage, a finding consistent with that described in other reports (22,23). Overexpression of *Runx*1 in chondrocytes does not induce any phenotypic abnormalities in the growth-plate chondrocyte, suggesting that Runx1 does not play a major role in the differentiation of these chondrocytes. Interestingly, it has been reported that forced expression of *Runx*1 in mesenchymal cells induced chondrocyte differentiation in vitro (24). This indicates that the function of Runx1 is possibly required only in the very early stages of chondrocyte differentiation. However, because the present study used an α1(II) collagen promoter to drive *Runx*1 expression, and this promoter is active only in cells that have differentiated into chondrocytes, we were precluded from testing this possibility.

Our results also showed that in WT mice, *Runx*3 was expressed in prehypertrophic chondrocytes and, in contrast to *Runx*2, its expression did not decrease throughout embryonic development, suggesting that *Runx*3 may play a role in chondrocyte differentiation after birth (8,9). Previously, Runx3, in conjunction with Runx2, was shown to regulate chondrocyte differentiation, but the neonatal mortality of Runx3-deficient mice hampered any further study of the role of Runx3 in the postnatal period (9). We recently observed that Runx3-deficient mice that survived perinatally exhibited impaired longitudinal growth postnatally (Takeda S, et al: unpublished observations). This observation, together with the ectopic mineralization in α1(II)-*Runx*3 mice, substantiates the physiologic importance of Runx3 in chondrocyte differentiation.

The results from the present study also showed that each member of the Runx family has a distinct ability to drive chondrocyte differentiation in vivo. Notably, only the α1(II)-*Runx*2 mice developed the phenotypes of both ectopic mineralization and IVD degeneration. This ability of Runx2 to induce both intervertebral degeneration and growth-plate chondrocyte differentiation could be attributable to its unique expression pattern or to its ability to recruit specific coregulators. The latter explanation is more likely, since the Runx-transgenic mice had distinct phenotypes despite comparable patterns of expression and comparable levels of each transgene driven by the same promoter cassette in each mouse. Since the runt DNA binding domain was observed to be highly homologous with that in other Runx proteins (Figure 2A), and yet the α1(II)-*Runx*2ΔQA mice still exhibited ectopic chondrocyte differentiation (Figure 2D), it is conceivable that the carboxyl domain

of Runx2 may interact with specific coregulators to induce chondrocyte differentiation.

Indeed, many transcriptional regulators have been found to be associated with the C-terminus of Runx2 (25–29). Of these regulators, Smad3 is the most promising, since Runx2, but not Runx1 or Runx3, has been shown to induce osteocalcin promoter activity, and this was inhibited by activation of transforming growth factor β (TGFβ) or Smad3 (30,31). Moreover, mice that either expressed a dominant-negative form of the TGFβII receptor or were deficient in Smad3 developed accelerated chondrocyte differentiation as well as kyphosis (32,33), which is reminiscent of the phenotype observed in α1(II)-*Runx*2 mice. Therefore, TGFβ/Smad3 signaling and Runx2 may cooperatively regulate chondrocyte differentiation. This hypothesis would be supported if Runx2 activity were shown to be increased either in mice expressing a dominant-negative form of the TGFβII receptor or in mice deficient in Smad3.

The most interesting and unexpected finding in the present study was the observation of IVD degeneration in both α1(II)-*Runx*1 and α1(II)-*Runx*2 mice. IVD degeneration is one of the most common degenerative disorders of the joints (34). Although matrix metalloproteinase 3 and a number of matrix genes, such as type II collagen, type IX collagen, and aggrecan, have been shown to be involved in the pathogenesis of IVD degeneration, the molecular mechanism is still largely unknown.

In this study, we demonstrated that Runx2 is involved in the development of IVD degeneration. There was substantial evidence to support this conclusion. First, overexpression of *Runx*2 or *Runx*1 in cartilaginous endplates induced IVD destruction. Second, weight loading, which is clinically a major cause of IVD degradation, induced expression of *Runx*2, but not that of *Runx*1, in the endplate of WT mice. Third, *Runx*2 expression coincided with the region of degradation of extracellular matrices in WT mice. We showed that Runx2 protein was expressed in older WT mice, but not in young mice; this coincided with the timeframe over which some of the WT mice developed IVD degradation. Finally, *Runx*2 expression was clearly induced in the degraded IVD in human patients.

Notably, the phenotypic abnormalities observed in α1(II)-*Runx*1– or α1(II)-*Runx*2–transgenic mice did not completely recapitulate the phenotype observed in human patients with IVD degeneration. Nevertheless, although the phenotype was much milder in mice with mechanical stress–induced IVD degeneration, it still led to concurrent expression of *Runx*2 in the mice. In fact, histologically, these mice exhibited degenerated nucleus pulposus without IVD height abnormalities, equivalent to the grade 3 to grade 4 IVD degeneration (17) observed in human patients. Collectively, our observations in mice and humans strongly support the hypothesis that Runx2 is intimately involved in IVD degradation and may even physiologically initiate the process.

The molecular mechanism by which mechanical loading induces expression of Runx2 in the IVD is unknown. However, it has been reported that mechanical loading induces Runx2 expression in osteoblasts through the MAP kinase pathway (35), and this same pathway may also be involved in the Runx2 expression observed in IVD degeneration. Given the prevalence of IVD degeneration in humans, an approach involving manipulation of the activity or expression of *Runx*2 or its downstream genes may be an attractive proposition as a novel therapy for these types of conditions.

ACKNOWLEDGMENTS

We would like to thank M. Patel, T. Kato, M. Noda, and U. Chung for helpful discussions and for reading the text. We also thank S. Sunamura and J. Chen for their superb technical assistance, and B. de Crombrugghe for providing the α1(II) collagen promoter and enhancer cassette.

AUTHOR CONTRIBUTIONS

Dr. Takeda had full access to all of the data in the study and takes responsibility for the integrity of the data and the accuracy of the data analysis.

Study design. Takeda.

Acquisition of data. Sato, Kimura, Ozdemir, Asou, Miyazaki, Jinno, Ae, Liu, Osaki, Takeuchi, Fukumoto, Kawaguchi, Haro, Shinomiya, Karsenty.

Analysis and interpretation of data. Takeda.

Manuscript preparation. Takeda.

Statistical analysis. Takeda.

REFERENCES

1. Kronenberg HM. Developmental regulation of the growth plate. Nature 2003;423:332–6.
2. Karsenty G, Wagner EF. Reaching a genetic and molecular understanding of skeletal development [review]. Dev Cell 2002;2: 389–406.
3. Poole AR. The growth plate: cellular physiology, cartilage assembly and mineralization. In: Hall BK, Newman SA, editors. Cartilage: molecular aspects. Boca Raton (FL): CRC Press; 1991. p. 179–211.
4. Bi W, Deng JM, Zhang Z, Behringer RR, de Crombrugghe B. Sox9 is required for cartilage formation. Nat Genet 1999;22:85–9.
5. Akiyama H, Chaboissier MC, Martin JF, Schedl A, de Crombrugghe B. The transcription factor Sox9 has essential roles in successive steps of the chondrocyte differentiation pathway and is required for expression of Sox5 and Sox6. Genes Dev 2002;16: 2813–28.
6. Ueta C, Iwamoto M, Kanatani N, Yoshida C, Liu Y, Enomoto-Iwamoto M, et al. Skeletal malformations caused by overexpres-

sion of Cbfa1 or its dominant negative form in chondrocytes. J Cell Biol 2001;153:87–100.
7. Takeda S, Bonnamy JP, Owen MJ, Ducy P, Karsenty G. Continuous expression of Cbfa1 in nonhypertrophic chondrocytes uncovers its ability to induce hypertrophic chondrocyte differentiation and partially rescues Cbfa1-deficient mice. Genes Dev 2001;15: 467–81.
8. Stricker S, Fundele R, Vortkamp A, Mundlos S. Role of Runx genes in chondrocyte differentiation. Dev Biol 2002;245:95–108.
9. Yoshida CA, Yamamoto H, Fujita T, Furuichi T, Ito K, Inoue K, et al. Runx2 and Runx3 are essential for chondrocyte maturation, and Runx2 regulates limb growth through induction of Indian hedgehog. Genes Dev 2004;18:952–63.
10. Ito Y, Miyazono K. RUNX transcription factors as key targets of TGF-β superfamily signaling. Curr Opin Genet Dev 2003;13:43–7.
11. Thirunavukkarasu K, Mahajan M, McLarren KW, Stifani S, Karsenty G. Two domains unique to the osteoblast-specific transcription factor Osf2/Cbfa1 contribute to its transactivation function and its inability to heterodimerize with Cbfβ. Mol Cell Biol 1998;18:4197–208.
12. Otto F, Thornell AP, Crompton T, Denzel A, Gilmour KC, Rosewell IR, et al. Cbfa1, a candidate gene for cleidocranial dysplasia syndrome, is essential for osteoblast differentiation and bone development. Cell 1997;89:765–71.
13. Van der Kraan PM, Vitters EL, van Beuningen HM, van de Putte LB, van den Berg WB. Degenerative knee joint lesions in mice after a single intra-articular collagenase injection: a new model of osteoarthritis. J Exp Pathol (Oxford) 1990;71:19–31.
14. Planaguma J, Diaz-Fuertes M, Gil-Moreno A, Abal M, Monge M, Garcia A, et al. A differential gene expression profile reveals overexpression of RUNX1/AML1 in invasive endometrioid carcinoma. Cancer Res 2004;64:8846–53.
15. Osaki M, Moriyama M, Adachi K, Nakada C, Takeda A, Inoue Y, et al. Expression of RUNX3 protein in human gastric mucosa, intestinal metaplasia and carcinoma. Eur J Clin Invest 2004;34: 605–12.
16. Lotz JC, Colliou OK, Chin JR, Duncan NA, Liebenberg E. Compression-induced degeneration of the intervertebral disc: an in vivo mouse model and finite-element study. Spine 1998;23: 2493–506.
17. Pfirrmann CW, Metzdorf A, Zanetti M, Hodler J, Boos N. Magnetic resonance classification of lumbar intervertebral disc degeneration. Spine 2001;26:1873–8.
18. Mundlos S. Expression patterns of matrix genes during human skeletal development. Prog Histochem Cytochem 1994;28:1–47.
19. Zhou G, Lefebvre V, Zhang Z, Eberspaecher H, de Crombrugghe B. Three high mobility group-like sequences within a 48-base pair enhancer of the Col2a1 gene are required for cartilage-specific expression in vivo. J Biol Chem 1998;273:14989–97.
20. McLeod MJ. Differential staining of cartilage and bone in whole mouse fetuses by alcian blue and alizarin red S. Teratology 1980;22:299–301.
21. Urban JP, Roberts S. Degeneration of the intervertebral disc. Arthritis Res Ther 2003;5:120–30.
22. Smith N, Dong Y, Lian JB, Pratap J, Kingsley PD, van Wijnen AJ, et al. Overlapping expression of Runx1(Cbfa2) and Runx2(Cbfa1) transcription factors supports cooperative induction of skeletal development. J Cell Physiol 2005;203:133–43.
23. Yamashiro T, Aberg T, Levanon D, Groner Y, Thesleff I. Expression of Runx1, -2 and -3 during tooth, palate and craniofacial bone development. Mech Dev 2002;119 Suppl 1:S107–10.
24. Wang Y, Belflower RM, Dong YF, Schwarz EM, O'Keefe RJ, Drissi H. Runx1/AML1/Cbfa2 mediates onset of mesenchymal cell differentiation toward chondrogenesis. J Bone Miner Res 2005;20: 1624–36.
25. Xiao G, Jiang D, Ge C, Zhao Z, Lai Y, Boules H, et al. Cooperative interactions between activating transcription factor 4 and Runx2/Cbfa1 stimulate osteoblast-specific osteocalcin gene expression. J Biol Chem 2005;280:30689–96.
26. Wang W, Wang YG, Reginato AM, Glotzer DJ, Fukai N, Plotkina S, et al. Groucho homologue Grg5 interacts with the transcription factor Runx2-Cbfa1 and modulates its activity during postnatal growth in mice. Dev Biol 2004;270:364–81.
27. Gutierrez S, Javed A, Tennant DK, van Rees M, Montecino M, Stein GS, et al. CCAAT/enhancer-binding proteins (C/EBP) β and δ activate osteocalcin gene transcription and synergize with Runx2 at the C/EBP element to regulate bone-specific expression. J Biol Chem 2002;277:1316–23.
28. Thomas DM, Carty SA, Piscopo DM, Lee JS, Wang WF, Forrester WC, et al. The retinoblastoma protein acts as a transcriptional coactivator required for osteogenic differentiation. Mol Cell 2001; 8:303–16.
29. Zhang YW, Yasui N, Ito K, Huang G, Fujii M, Hanai J, et al. A RUNX2/PEBP2α A/CBFA1 mutation displaying impaired transactivation and Smad interaction in cleidocranial dysplasia. Proc Natl Acad Sci U S A 2000;97:10549–54.
30. Alliston T, Choy L, Ducy P, Karsenty G, Derynck R. TGF-β-induced repression of CBFA1 by Smad3 decreases cbfa1 and osteocalcin expression and inhibits osteoblast differentiation. EMBO J 2001;20:2254–72.
31. Kang JS, Alliston T, Delston R, Derynck R. Repression of Runx2 function by TGF-β through recruitment of class II histone deacetylases by Smad3. EMBO J 2005;24:2543–55.
32. Serra R, Johnson M, Filvaroff EH, LaBorde J, Sheehan DM, Derynck R, et al. Expression of a truncated, kinase-defective TGF-β type II receptor in mouse skeletal tissue promotes terminal chondrocyte differentiation and osteoarthritis. J Cell Biol 1997; 139:541–52.
33. Yang X, Chen L, Xu X, Li C, Huang C, Deng CX. TGF-β/Smad3 signals repress chondrocyte hypertrophic differentiation and are required for maintaining articular cartilage. J Cell Biol 2001;153: 35–46.
34. Powell MC, Wilson M, Szypryt P, Symonds EM, Worthington BS. Prevalence of lumbar disc degeneration observed by magnetic resonance in symptomless women. Lancet 1986;2:1366–7.
35. Ziros PG, Gil AP, Georgakopoulos T, Habeos I, Kletsas D, Basdra EK, et al. The bone-specific transcriptional regulator Cbfa1 is a target of mechanical signals in osteoblastic cells. J Biol Chem 2002;277:23934–41.

ARTHRITIS & RHEUMATISM
Vol. 56, No. 10, October 2007, pp 3358–3365
DOI 10.1002/art.22941

Prevention of Cartilage Destruction With Intraarticular Osteoclastogenesis Inhibitory Factor/Osteoprotegerin in a Murine Model of Osteoarthritis

Sadanori Shimizu,[1] Yoshinori Asou,[1] Soichiro Itoh,[1] Ung-il Chung,[2] Hiroshi Kawaguchi,[2] Kenichi Shinomiya,[1] and Takeshi Muneta[1]

Objective. **To investigate the effect of osteoclastogenesis inhibitory factor/osteoprotegerin (OPG) on chondrocytes in the development of osteoarthritis (OA) in vivo.**

Methods. **To determine the role of endogenous OPG in the progression of OA, OA was surgically induced in $OPG^{+/-}$ mice and their wild-type (WT) littermates. To determine the role of exogenous OPG, knee joints of C57BL/6J mice with surgically induced OA were injected intraarticularly with recombinant human OPG (rHuOPG) or vehicle 5 times a week. All mice were euthanized 4 weeks after OA induction; joints were harvested and evaluated immunohistochemically.**

Results. **Although OA changes were induced in both WT and $OPG^{+/-}$ mice, the degenerative changes in the articular cartilage were significantly enhanced in $OPG^{+/-}$ mice. In C57BL/6J mice with surgically induced OA, intraarticular OPG administration protected the articular cartilage from the progression of OA. The Mankin and cartilage destruction scores in OPG-treated animals were ~50% of those seen in the control group. Furthermore, OPG administration significantly protected articular cartilage thickness. Findings of the TUNEL assay indicated that rHuOPG prevented chondrocyte apoptosis in joints with surgically induced OA. Results of immunostaining indicated that OPG protein was detected in the synovium and in resident chondrocytes at higher levels in the OPG-treated group than in the control group.**

Conclusion. **These data indicate that endogenous OPG had a protective effect against the cartilage destruction that occurs during OA progression. Furthermore, direct administration of rHuOPG to articular chondrocytes prevented cartilage destruction in an experimental murine model of OA via prevention of chondrocyte apoptosis.**

Osteoarthritis (OA), a chronic degenerative joint disorder characterized by articular cartilage destruction and osteophyte formation, is a major cause of disability worldwide (1). OA risk factors identified by previous epidemiologic studies are age, history of trauma, occupation, and sex. Since these factors are closely related to the mechanical load placed on joints, OA is thought to be induced primarily by accumulated mechanical stress (2). Although several symptomatic therapies have been attempted for OA, no radical treatment methods have been established, with the exception of arthroplasty. In OA, articular chondrocytes appear to be eliminated by apoptosis (2,3). The number of apoptotic cells in the articular cartilage of OA patients was found to be significantly higher than the number in healthy subjects (4). In addition, chondrocyte apoptosis has been reproduced in animals with experimentally induced OA (5).

Osteoclastogenesis inhibitory factor/osteoprotegerin (OPG) is a heparin-binding basic glycoprotein that was originally purified from the conditioned medium of the human embryonic lung fibroblast line IMR-90 (6). OPG is a secreted member of the tumor

Supported by Daiichi Sankyo Co., Ltd. Drs. Shimizu, Shinomiya, and Muneta's work was supported by the Center of Excellence Program for Frontier Research on Molecular Destruction and Reconstruction of Tooth and Bone, Tokyo Medical and Dental University.

[1]Sadanori Shimizu, MD, Yoshinori Asou, MD, PhD, Soichiro Itoh, MD, PhD, Kenichi Shinomiya, MD, PhD, Takeshi Muneta, MD, PhD: Tokyo Medical and Dental University, Tokyo, Japan; [2]Ung-il Chung, MD, PhD, Hiroshi Kawaguchi, MD, PhD: University of Tokyo, Tokyo, Japan.

Dr. Asou is submitting a patent application for an adaptation of osteoprotegerin.

Address correspondence and reprint requests to Yoshinori Asou, MD, PhD, Tokyo Medical and Dental University, Department of Orthopedic Surgery, 1-5-45 Yushima, Bunkyo-ku, Tokyo 113-8519, Japan. E-mail: aso.orth@tmd.ac.jp.

Submitted for publication January 8, 2007; accepted in revised form June 29, 2007.

necrosis factor (TNF) receptor family that functions as a decoy receptor for RANKL (6–8), serving to inhibit osteoclastogenesis and accelerate osteoclast apoptosis (9,10). OPG deficiency in mice causes severe bone loss and destruction of internal bone structures through an unbalanced shift in favor of osteoclast differentiation, but without other abnormalities (11–13). Homozygous OPG knockout ($OPG^{-/-}$) mice also exhibit unusual bone formations associated with severe destruction of growth plate cartilage (14,15). The proximal epiphyses of the femurs and humeri in $OPG^{-/-}$ mice exhibit resorption of subchondral bone and collapse of the joint surface resulting from mechanical damage at the end of the bone (13). Inactivating mutations in *TNFRSF11B*, the gene that encodes OPG, result in juvenile Paget's disease (16). Polymorphisms in OPG also increase the risk of developing Paget's disease (16). Patients with Paget's disease exhibit a wide range of clinical manifestations, including bone pain, fracture, hearing loss, syndromes of neurologic compression, and secondary OA (17).

RANK, RANKL, and OPG messenger RNA (mRNA) and proteins are expressed in normal cartilage. Cartilage from patients with OA contains increased levels of OPG mRNA, and the expression of these 3 proteins extends into the midzone of the cartilage (18,19). OPG is expressed in the synovial tissues of patients with rheumatoid arthritis, spondylarthropathies, and OA (19). OPG expression by chondrocytes is increased in response to in vitro stimulation with interleukin-1β, the proinflammatory cytokine expressed in OA joints (18), implying the existence of OPG targets within the joint space, in addition to the subchondral area.

The function of OPG that is expressed during OA pathogenesis is poorly understood. In this study, we investigated the effects of OPG on chondrocytes during OA development in vivo. We demonstrated that endogenous OPG functions in the prevention of articular cartilage degradation in a mechanical stress–induced animal model of OA. Furthermore, we found that direct administration of exogenous OPG to articular chondrocytes effectively retarded the progression of OA via suppression of chondrocyte apoptosis.

MATERIALS AND METHODS

Animals. C57BL/6J mice (8–10 weeks old) were purchased from Sankyo Labo (Tokyo, Japan). Mice heterozygous for the OPG gene mutation, OPG/Jcl, on a C57BL/6J background were purchased from Japan Clea (Tokyo, Japan).

Surgical induction of OA. All experiments were performed according to a protocol approved by the Animal Care and Use Committee of Tokyo Medical and Dental University. With the mice under general anesthesia, the right knee joint was surgically exposed. The medial collateral ligament was transected, and the medial meniscus was removed using a surgical microscope with microsurgical technique, as previously reported (1). The left knee joint was sham-operated, without ligament transection or meniscectomy.

Reagents. Recombinant human OPG (rHuOPG) was kindly provided by Biological Research Laboratories, Daiichi Sankyo (Tokyo, Japan).

Experimental design. *Surgical induction of OA in $OPG^{+/-}$ mice.* $OPG^{+/-}$ mice (n = 7) and their wild-type (WT) littermates (n = 7) (ages 8–12 weeks) were surgically induced to develop OA by medial collateral ligament transection and medial meniscectomy. Four weeks after surgery, the mice were euthanized.

Intraarticular administration of rHuOPG. After surgical induction of OA, C57BL/6J mice (n = 14) were divided into 2 groups. The OPG-treated group (n = 7) was administered 100 ng of rHuOPG in 10 μl of phosphate buffered saline (PBS) intraarticularly 5 days a week beginning on postoperative day 1 and continuing for 4 weeks after the operation. The control group (n = 7) received 10 μl of PBS intraarticularly according to the same schedule as in the OPG-treated group. Four weeks after surgery, the animals were euthanized.

Assessment of the severity of OA. Whole knee joints were removed by dissection, fixed in 4% paraformaldehyde, and decalcified in EDTA. After dehydration and paraffin embedding, we cut serial 5-μm sagittal sections from the whole medial compartment of the joint. Two sections obtained at 100-μm intervals from the weight-bearing region of each knee joint were stained with Safranin O–fast green. OA severity in the tibial plateau was evaluated according to Mankin's histologic grading system (20,21), and a cartilage destruction score was also assigned (1). The thickness of the articular cartilage layer was measured as the average distance from the superficial layer to the osteochondral junction of the tibia. Quantitative determination of the articular cartilage thickness and bone volume in subchondral bone was made using Image-Pro Plus 4.1 software (Media Cybernetics, Carlsbad, CA).

Immunohistochemical analysis. Expression of OPG and TRAIL at the protein level was examined by immunohistochemistry using an anti-mouse OPG antibody (N-20; catalog no. sc-8468) or an anti-mouse TRAIL antibody (K-18; catalog no. sc-6079) according to the manufacturer's instructions (Santa Cruz Biotechnology, Santa Cruz, CA). Briefly, sections were blocked with 5% normal rabbit serum for 30 minutes, then incubated overnight with anti-mouse OPG antibody (1:100 dilution) or with anti-mouse TRAIL antibody (1:20 dilution) at 4°C in a humidified chamber. Sections were incubated for 30 minutes at room temperature with a biotinylated rabbit anti-goat IgG and visualized by peroxidase-conjugated avidin and diaminobenzidine using a Vectastain kit (Vector, Burlingame, CA).

TUNEL assay. The TUNEL assay was performed using a TUNEL detection kit according to the manufacturer's instructions (Takara Shuzo, Kyoto, Japan). Briefly, sections were incubated with 15 μg/ml of proteinase K for 15 minutes at room temperature, then washed with PBS. Endogenous peroxidase was inactivated with 3% H_2O_2 for 5 minutes at room temperature. After washing with PBS, sections were immersed

in buffer containing deoxynucleotidyl transferase and biotinylated dUTP and incubated for 90 minutes at 37°C in a humid atmosphere. After washing in PBS, signals were examined by fluorescence microscopy.

Statistical analysis. Data are expressed as the mean ± SD. Statistical analysis was performed with the Mann-Whitney U test. P values less than 0.05 were considered significant.

RESULTS

Enhancement of cartilage destruction by OPG heterozygous deficiency in an experimental OA model. To determine the role of endogenous OPG in the progression of OA, we compared histologic features in the knee joints of OPG-deficient mice with those in their WT littermates. Histologic sections of the knee joints of young adult homozygous OPG-knockout ($OPG^{-/-}$) mice (8 weeks old) exhibited significantly thinned articular cartilage layers, active infiltration of vessels into subchondral bone, and irregularity of the osteochondral junction as compared with knee joints from $OPG^{+/-}$ mice and WT littermates (Figures 1A–C). With aging, cartilage degradation was found to be enhanced in $OPG^{-/-}$ mice and even in $OPG^{+/-}$ mice (Figures 1D–F), which suggests that sufficient levels of OPG expression are essential for the prevention of age-dependent cartilage degradation. However, it was unclear whether OPG affected chondrocyte metabolism directly or whether it was affected indirectly through osteoclastic erosion of subchondral bone via RANK signaling, since subchondral bone was apparently reduced in $OPG^{-/-}$ mice.

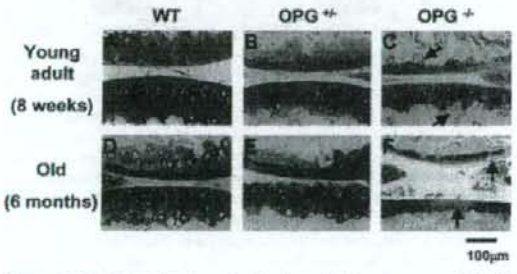

Figure 1. Histologic findings in the knee joints of young adult (8-week-old) and old (6-month-old) osteoprotegerin (OPG)–deficient mice and their wild-type (WT) littermates. Compared with the $OPG^{+/-}$ (**B**) and WT (**A**) littermates at 8 weeks of age, the $OPG^{-/-}$ mice (**C**) exhibited thinning of the articular cartilage layers, active infiltration of vessels into subchondral bone (**arrows**), and irregularity of the osteochondral junction. At 6 months of age, signs of enhanced cartilage degradation were observed in the OPG-deficient mice, such as superficial fibrillation (**E**) (**arrowhead**) and proteoglycan defects (**F**) (**arrows**), as compared with their WT littermates (**D**).

Therefore, we used young adult $OPG^{+/-}$ mice in our experimental model of OA to avoid the effect of the subchondral bone defect and to examine the effects of OPG insufficiency on cartilage.

We compared the rates of progression and the severity of OA in $OPG^{+/-}$ mice subjected to medial collateral ligament transection and medial meniscectomy to induce OA (1) with those in their WT littermates. Both the structure of the articular cartilage and the total bone volume were similar in $OPG^{+/-}$ mice and WT littermates at the ages examined (8–12 weeks old). Mice were euthanized 4 weeks after the operation, and the knee joints were harvested and evaluated histologically.

Destruction of the medial tibial cartilage was observed in WT littermates, as reported previously (1) (Figure 2A, parts a and c). Histologic evaluation revealed that degenerative changes of the articular cartilage were enhanced in $OPG^{+/-}$ mice as compared with WT littermates (Figure 2A, parts b and d). Both the Mankin scores (Figure 2B) and the cartilage destruction scores (Figure 2C) in $OPG^{+/-}$ mice were 25% higher than those in the WT littermates ($P < 0.05$). The morphology of subchondral bone structures was not affected by OPG haploinsufficiency (Figure 2A, parts c and d). Cartilage thickness, however, was significantly reduced ($P < 0.05$) in $OPG^{+/-}$ mice (Figure 2D), indicating that endogenous OPG plays an important role in the maintenance of articular cartilage during the development of mechanical stress–induced OA.

Prevention of cartilage destruction in an experimental OA model by exogenous OPG administration. To examine whether exogenous OPG prevents cartilage destruction independently of the protection of subchondral bone structures, we administered rHuOPG by intraarticular injection to induce OA surgically in C57BL/6J mice. We chose this method because systemic administration of OPG may affect subchondral bone metabolism via the suppression of osteoclastogenesis. Medial collateral ligament transection and medial meniscectomy to induce OA were performed on the right knees of all mice; sham operations were performed on the left knees. OPG or vehicle alone was injected intraarticularly 5 days a week beginning the day after the operation, and all mice were euthanized 4 weeks after the operation.

Histologic investigation indicated that OPG administration protected the articular cartilage from proteoglycan depletion, alterations of surface structure, and

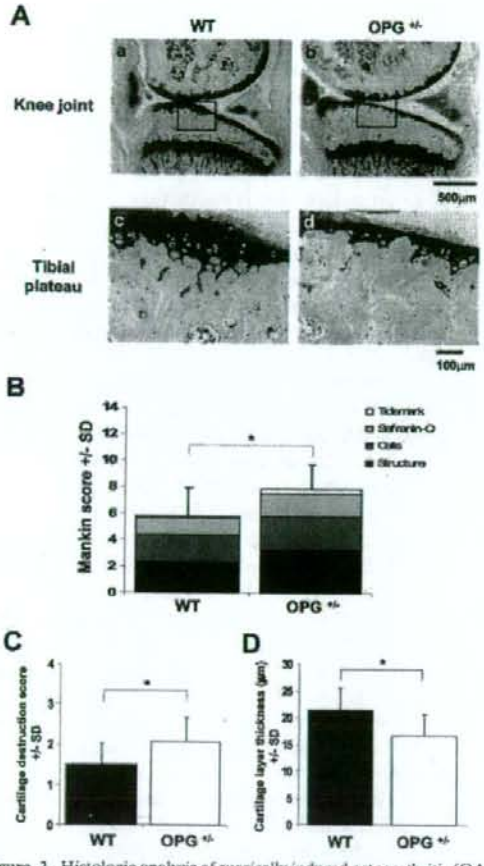

Figure 2. Histologic analysis of surgically induced osteoarthritis (OA) in the knee joints of young adult osteoprotegerin (OPG)–deficient mice and their wild-type (WT) littermates. OA was surgically induced in mice ages 8–12 weeks, and knee joints were harvested 4 weeks later. A, Sections of articular cartilage from WT (a and c) and $OPG^{+/-}$ (b and d) mice were stained with Safranin O to detect proteoglycans. Degenerative changes in the articular cartilage were enhanced in $OPG^{+/-}$ mice (b) as compared with their WT littermates (a). Morphologic features of the subchondral bone were similar in the WT (c) and $OPG^{+/-}$ (d) mice. Boxed and labeled areas in a and b are shown at higher magnification in c and d, respectively. B and C, Histologic changes in the OA joints were assigned Mankin scores (B) and cartilage destruction scores (C). Scores in the $OPG^{+/-}$ mice were 25% higher than those in their WT littermates. D, Mean cartilage thickness in OA joints was measured as the average distance from the superficial layer to the osteochondral junction of the tibia. The mean cartilage thickness was significantly reduced in $OPG^{+/-}$ mice as compared with their WT littermates. Values in B–D are the mean and SD of 7 mice per group. * = $P < 0.05$ by Mann-Whitney U test.

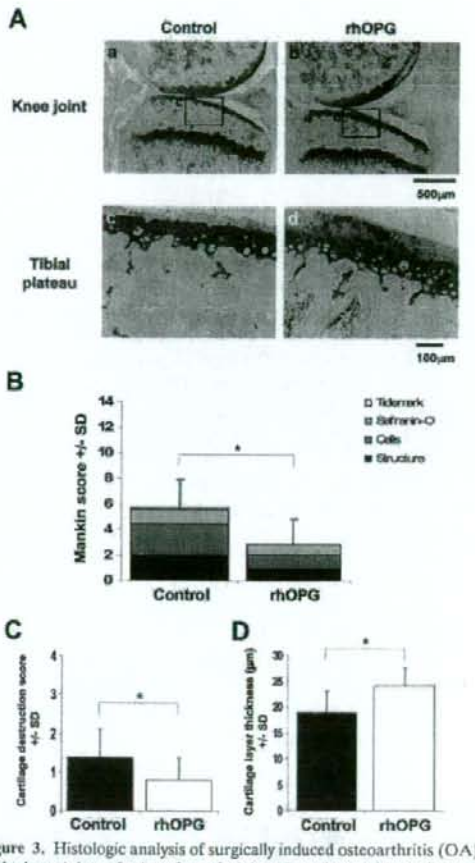

Figure 3. Histologic analysis of surgically induced osteoarthritis (OA) in the knee joints of mice after administration of recombinant human osteoprotegerin (rHuOPG) or vehicle. Intraarticular injection of rHuOPG (rhOPG) or vehicle alone (control) into mouse knee joints was performed 5 times a week beginning the day after surgery and continuing for 4 weeks thereafter. A, Sections of articular cartilage from the knee joints of control (a and c) or OPG-treated (b and d) mice were stained with Safranin O to detect proteoglycans. Degenerative changes in the articular cartilage were reduced in OPG-treated mice as compared with the controls (a–d). Morphologic features of the subchondral bone were similar in the control (c) and OPG-treated (d) mice. Boxed and labeled areas in a and b are shown at higher magnification in c and d, respectively. B and C, Histologic changes in the OA joints were assigned Mankin scores (B) and cartilage destruction scores (C). Scores in the OPG-treated mice were less than 50% of those in the controls. D, Mean cartilage thickness in OA joints was measured as the average distance from the superficial layer to the osteochondral junction of the tibia. The mean cartilage thickness was significantly reduced in the OPG-treated group as compared with the controls. Values in B–D are the mean and SD of 7 mice per group. * = $P < 0.05$ by Mann-Whitney U test.

clustering of chondrocytes (Figure 3A, parts a–d). At this time point, Mankin scores (Figure 3B) and cartilage destruction scores (Figure 3C) in OPG-treated animals were ~50% of those seen in the control group ($P < 0.05$). Thus, OPG administration significantly protected the articular cartilage thickness (Figure 3D). The structure and bone volume (mean ± SD bone volume/total volume 56.79 ± 12% in the control group versus 59.18 ± 22% in the OPG-treated group) of subchondral bone were not affected by intraarticular administration of OPG, as was expected (Figure 3A, parts c and d). The number of osteoclasts in the subchondral region (mean ± SD 4.4 ± 1.1/mm in the control group versus 4.4 ± 1.2/mm in the OPG-treated group) was also similar between these groups, indicating that exogenous OPG protected the articular cartilage from degradation in a manner that was independent of the protection of subchondral bone.

Prevention of chondrocyte apoptosis in an experimental OA model by exogenous OPG administration. Chondrocyte apoptosis is increased in OA cartilage and is anatomically linked to proteoglycan depletion (2,3). These observations prompted us to investigate the effect of OPG administration on chondrocyte apoptosis. We injected rHuOPG or vehicle alone into the knee joints of C57BL/6J mice with surgically induced OA for 5 days a week beginning on postoperative day 1 and continuing for 4 weeks. Knee joints were then examined after TUNEL staining. TUNEL-positive cells were abundant among the chondrocytes present in control mice with surgically induced OA that had received only PBS injection (Figure 4A, part a). In contrast, TUNEL-positive cells were rare in joints injected with rHuOPG (Figure 4A, part b). The number of TUNEL-positive chondrocytes in the joints of the OPG-treated group was almost one-third of that in the control group ($P < 0.05$) (Figure 4B). These data indicated that the anti-apoptotic effect of OPG functions to protect the articular cartilage.

Expression of OPG and TRAIL in chondrocytes of mice with experimentally induced OA. Immunohistochemical analysis indicated that while OPG could be detected in synovial cells and chondrocytes, OPG protein was observed at higher levels in the peripheral layers of OA joint cartilage and synovial tissue following OPG administration (Figure 5A). One of the OPG ligands, TRAIL, has also been observed in chondrocytes and synovial tissues from OA joints (18,19,22). Moreover, TRAIL is known to induce chondrocyte apoptosis in vitro (22,23). Our immunohistochemical analysis also

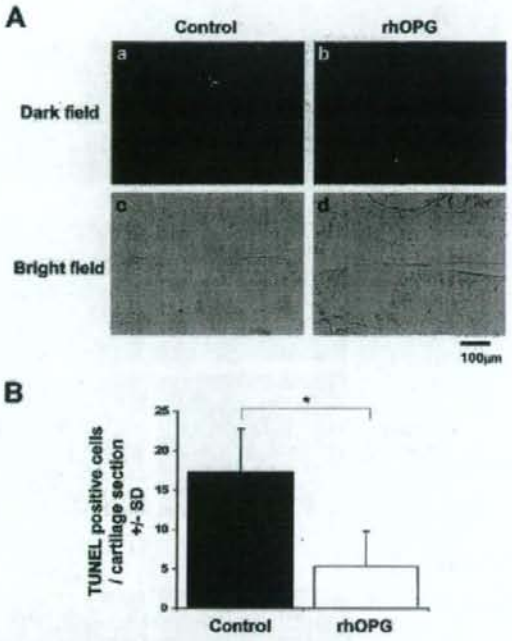

Figure 4. Analysis of apoptosis in TUNEL-stained sections of cartilage from mice with surgically induced osteoarthritis (OA) after intraarticular administration of recombinant human osteoprotegerin (rHuOPG) or vehicle. Intraarticular injection of rHuOPG (rhOPG) or vehicle alone (control) into mouse knee joints was performed 5 times a week beginning the day after surgery and continuing for 4 weeks thereafter. **A,** TUNEL staining of OA cartilage sections was examined by darkfield (**a** and **b**) and brightfield (**c** and **d**) microscopy. The number of TUNEL-positive cells was increased in knee joint cartilage from control mice (**a**) but was significantly reduced in knee joint cartilage from mice injected with rHuOPG (**b**). **B,** The number of TUNEL-positive cells per section of OA cartilage was determined under fluorescence microscopy. Values are the mean and SD of 5 mice per group. * = $P < 0.05$ by Mann-Whitney U test.

indicated that TRAIL was expressed in chondrocytes. TRAIL-positive chondrocytes were primarily detected in the periphery of the joint cartilage in OPG-treated animals (Figure 5B, part b), whereas they were present in the middle and deep zones of the joint cartilage, with hypertrophic differentiation, in control animals (Figure 5B, part a). The expression patterns of OPG and TRAIL overlapped significantly in the OPG-treated group (Figure 5A, part f, and Figure 5B, part b). These results suggest that exogenous OPG protected the articular chondrocytes by inhibiting TRAIL-induced apoptosis in vivo.

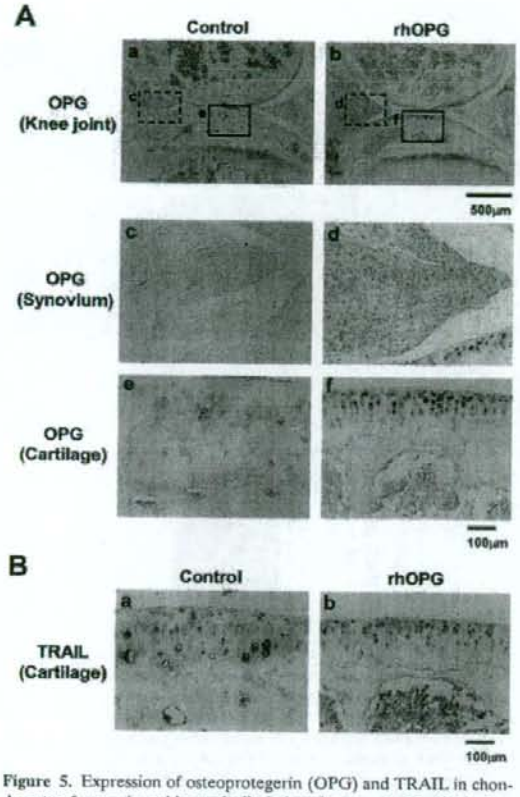

Figure 5. Expression of osteoprotegerin (OPG) and TRAIL in chondrocytes from mice with surgically induced osteoarthritis (OA) after intraarticular administration of recombinant human osteoprotegerin (rHuOPG) or vehicle. Intraarticular injection of rHuOPG (rhOPG) or vehicle alone (control) into mouse knee joints was performed 5 times a week beginning the day after surgery and continuing for 4 weeks thereafter. **A,** OPG protein was present at high levels in synovial cells (**d**) and cartilage chondrocytes (**f**) in sections from rHuOPG-treated mice, whereas only trace amounts of OPG protein were observed in control animals (**a**, **c**, and **e**). Control chondrocytes (**e**) showed hypertrophic changes as a result of OA progression, as compared with chondrocytes from rHuOPG-treated mice (**f**). Boxed and labeled areas in **a** and **b** are shown at higher magnification in **c** and **e** and in **d** and **f**, respectively. **B,** TRAIL expression was also observed in the cartilage chondrocytes of control (**a**) and OPG-treated (**b**) mice with surgically induced OA.

DISCUSSION

This study revealed the effects of reductions of endogenous OPG activity on the progression of instability-induced cartilage destruction in mice heterozygous for an OPG gene mutation. Previous studies have indicated that $OPG^{-/-}$ mice demonstrate severe destruction of growth plate cartilage and growth plate cartilage loss–induced epiphyseal and metaphyseal trabecular bone formation (14,15). Histologic examination revealed that at 8 weeks of age, $OPG^{-/-}$ mice exhibited irregular articular cartilage, including markedly thinned cartilage layers and invasion of the vasculature into the calcified layer (Figure 1C); in contrast, the articular cartilage of young adult $OPG^{+/-}$ mice was intact at this age (Figure 1B). Although $OPG^{+/-}$ mice exhibit a significant loss of total bone density compared with their WT littermates by the age of 6 months (mean ± SD 487.6 ± 27 mg/cm^3 versus 521.2 ± 29 mg/cm^3; $P < 0.05$), bone volume is comparable in young adult $OPG^{+/-}$ and WT mice at the ages evaluated in these experiments (13).

Since subchondral bone metabolism is important for the maintenance of articular cartilage (24), we chose young adult $OPG^{+/-}$ mice as our experimental OA model in which to examine the effects of OPG haploinsufficiency in chondrocytes on cartilage metabolism. After induction of OA in $OPG^{+/-}$ mice and their WT littermates, the $OPG^{+/-}$ mice exhibited severe articular cartilage degeneration as compared with the WT mice. This observation indicated that adequate OPG was required for the maintenance of cartilage and the prevention of mechanical stress–induced cartilage degeneration. The observation that the subchondral bone structures in $OPG^{+/-}$ mice and their WT littermates were histologically indistinguishable suggested that endogenous OPG likely plays only a minimal role in subchondral bone turnover in the acute phase of OA progression.

We also demonstrated that intraarticular administration of exogenous OPG effectively protected the articular cartilage from degradation. Although previous reports suggested a protective effect of OPG on cartilage in arthritis models, systemically administered OPG protected both the articular cartilage and articular bone (25–28). Therefore, it was unclear whether in arthritis, OPG affected chondrocyte metabolism directly or indirectly through osteoclastic bone erosion of subchondral bone via RANK signaling (27). To study this, we administered rHuOPG intraarticularly, which revealed the direct effect of this substance on articular chondrocyte metabolism.

TRAIL, one of the ligands for OPG, was also expressed in chondrocytes, as reported previously (22), regardless of OPG administration. OPG binds to TRAIL, a death domain–containing type II transmembrane protein member of the TNF superfamily (29,30). TRAIL constitutes a family of ligands that transduces death signals through a death domain–containing receptor (31). OPG inhibits TRAIL-induced apoptosis in

Jurkat cells (29) and endothelial cells (32). TRAIL also induces chondrocyte apoptosis in vitro; its expression is increased in the chondrocytes of rats with experimentally induced OA (22). In this study, OPG was observed in TRAIL-expressing chondrocytes and synovium in OPG-treated animals. These findings are consistent with the hypothesis that exogenously administered OPG prevents chondrocyte apoptosis in our model of surgically induced OA. Although inhibition of the TRAIL pathway by OPG may be one of the potent mechanisms of OA prevention of OPG, the target of OPG is still to be elucidated.

The concentration of OPG we used was determined according to previous observations in endothelial cells (32), where endothelial cell apoptosis induced by serum deprivation was blocked by OPG concentrations >0.5 μg/ml. The appropriate concentration of OPG will need to be determined for any future clinical applications.

TUNEL staining revealed that OPG administration significantly suppressed chondrocyte apoptosis. Exogenous OPG was confined to the cartilage and synovium; the subchondral bone volume and vascular invasion were not affected by intraarticular OPG administration. These observations indicated that the chondroprotective effect of OPG was independent of the subchondral bone protection.

To investigate the function of OPG in articular chondrocyte metabolism, we used an experimental stress-induced murine model of OA that is reproducible and closely resembles OA in humans (1). The combination of medial collateral ligament transection and medial meniscectomy induced medial tibial cartilage destruction within 4 weeks. The early changes in the articular cartilage after surgery resulted from a defect in the superficial zone and corresponded to a decrease in Safranin O staining. These initial findings were followed by progressive cartilage destruction in a manner identical to that reported for OA pathology in humans as determined by arthroscopic and histologic analyses (33,34). Along with the catabolic changes, the anabolic reactions of chondrocyte proliferation and subchondral sclerosis were also observed in our model.

The findings of this study cannot rule out the importance of subchondral bone metabolism in articular cartilage protection. Although articular chondrocytes do not have an intact RANK signaling apparatus, RANKL-deficient mice have been shown to be protected from bone erosion in a serum-transfer model of arthritis (35), indicating that OPG protects articular cartilage via maintenance of subchondral bone. In the rat inflammatory arthritis model, systemic administration of OPG preserved articular cartilage (25,27). While significant chondroprotection was observed in mildly inflamed joints following administration of Fc-OPG, no significant protection was seen in the more severely inflamed joints of rats treated with OPG. Similarly, in a serum-transfer model of arthritis, RANKL-deficient mice exhibited cartilage loss despite protection from bone erosion and despite partial inhibition of cartilage destruction (35). In these experiments, OPG was administered systemically; intraarticular OPG levels were not affected (27). Administration of OPG both systemically and intraarticularly may have an additive effect on chondrocyte protection in arthritis.

Bone resorption inhibitors, including bisphosphonates and calcitonin, have been shown to reduce cartilage degradation in experimental arthritis models (36,37). In a rat model of stress-induced OA, alendronate was shown to have a partial chondroprotective effect during the early stages of disease (36). Although the direct target of bisphosphonates is not known, bisphosphonate inhibition of subchondral bone turnover may be a candidate mechanism that would explain this phenomenon. Bisphosphonates may indirectly reduce cartilage breakdown by altering the distribution of mechanical stress. Bisphosphonate inhibition of osteoclastic bone resorption may also reduce the release of inflammatory cytokines and growth factors (36).

In conclusion, we have demonstrated that rHuOPG prevents cartilage destruction in an experimental murine model of OA and that endogenous OPG protects against cartilage destruction during the progression of OA. Our results provide clues that OPG prevents chondrocyte apoptosis via a direct effect on chondrocytes in vivo. These results support a potential therapeutic application of rHuOPG in human OA.

ACKNOWLEDGMENTS

The authors would like to acknowledge Dr. Satoru Kamekura for technical advice with the experimental OA model and Miyoko Ojima for expert help with the histologic analyses.

AUTHOR CONTRIBUTIONS

Dr. Asou had full access to all of the data in the study and takes responsibility for the integrity of the data and the accuracy of the data analysis.

Study design. Asou, Chung, Kawaguchi.

Acquisition of data. Shimizu, Itoh.

Analysis and interpretation of data. Asou, Chung, Kawaguchi, Muneta.

Manuscript preparation. Shimizu, Asou, Shinomiya.

Statistical analysis. Shimizu.

REFERENCES

1. Kamekura S, Hoshi K, Shimaoka T, Chung U, Chikuda H, Yamada T, et al. Osteoarthritis development in novel experimental mouse models induced by knee joint instability. Osteoarthritis Cartilage 2005;13:632–41.
2. Hashimoto S, Ochs RL, Komiya S, Lotz M. Linkage of chondrocyte apoptosis and cartilage degradation in human osteoarthritis. Arthritis Rheum 1998;41:1632–8.
3. Kim HA, Lee YJ, Seong SC, Choe KW, Song YW. Apoptotic chondrocyte death in human osteoarthritis. J Rheumatol 2000;27: 455–62.
4. Amin AR, Abramson SB. The role of nitric oxide in articular cartilage breakdown in osteoarthritis. Curr Opin Rheumatol 1998; 10:263–8.
5. Hashimoto S, Takahashi K, Amiel D, Coutts RD, Lotz M. Chondrocyte apoptosis and nitric oxide production during experimentally induced osteoarthritis. Arthritis Rheum 1998;41:1266–74.
6. Tsuda E, Goto M, Mochizuki S, Yano K, Kobayashi F, Morinaga T, et al. Isolation of a novel cytokine from human fibroblasts that specifically inhibits osteoclastogenesis. Biochem Biophys Res Commun 1997;234:137–42.
7. Yasuda H, Shima N, Nakagawa N, Yamaguchi K, Kinosaki M, Mochizuki S, et al. Osteoclast differentiation factor is a ligand for osteoprotegerin/osteoclastogenesis-inhibitory factor and is identical to TRANCE/RANKL. Proc Natl Acad Sci U S A 1998;95: 3597–602.
8. Yasuda H, Shima N, Nakagawa N, Mochizuki SI, Yano K, Fujise N, et al. Identity of osteoclastogenesis inhibitory factor (OCIF) and osteoprotegerin (OPG): a mechanism by which OPG/OCIF inhibits osteoclastogenesis in vitro. Endocrinology 1998;139: 1329–37.
9. Lacey DL, Tan HL, Lu J, Kaufman S, Van G, Qiu W, et al. Osteoprotegerin ligand modulates murine osteoclast survival in vitro and in vivo. Am J Pathol 2000;157:435–48.
10. Burr DB. Anatomy and physiology of the mineralized tissues: role in the pathogenesis of osteoarthrosis. Osteoarthritis Cartilage 2004;12 Suppl A: S20–30.
11. Yano K, Tsuda E, Washida N, Kobayashi F, Goto M, Harada A, et al. Immunological characterization of circulating osteoprotegerin/osteoclastogenesis inhibitory factor: increased serum concentrations in postmenopausal women with osteoporosis. J Bone Miner Res 1999;14:518–27.
12. Mizuno A, Amizuka N, Irie K, Murakami A, Fujise N, Kanno T, et al. Severe osteoporosis in mice lacking osteoclastogenesis inhibitory factor/osteoprotegerin. Biochem Biophys Res Commun 1998;247:610–5.
13. Bucay N, Sarosi I, Dunstan CR, Morony S, Tarpley J, Capparelli C, et al. Osteoprotegerin-deficient mice develop early onset osteoporosis and arterial calcification. Genes Dev 1998;12:1260–8.
14. Amizuka N, Shimomura J, Li M, Seki Y, Oda K, Henderson JE, et al. Defective bone remodelling in osteoprotegerin-deficient mice. J Electron Microsc (Tokyo) 2003;52:503–13.
15. Kawana F, Sasaki T. Osteoclast differentiation and characteristic trabecular bone formation during growth plate destruction in osteoprotegerin-deficient mice. J Electron Microsc (Tokyo) 2003; 52:515–25.
16. Daroszewska A, Ralston SH. Genetics of Paget's disease of bone. Clin Sci (Lond) 2005;109:257–63.
17. Van Staa TP, Selby P, Leufkens HG, Lyles K, Sprafka JM, Cooper C. Incidence and natural history of Paget's disease of bone in England and Wales. J Bone Miner Res 2002;17:465–71.
18. Komuro H, Olee T, Kuhn K, Quach J, Brinson DC, Shikhman A, et al. The osteoprotegerin/receptor activator of nuclear factor κB/receptor activator of nuclear factor κB ligand system in cartilage. Arthritis Rheum 2001;44:2768–76.
19. Haynes DR, Barg E, Crotti TN, Holding C, Weedon H, Atkins GJ, et al. Osteoprotegerin expression in synovial tissue from patients with rheumatoid arthritis, spondyloarthropathies and osteoarthritis and normal controls. Rheumatology (Oxford) 2003;42:123–34.
20. Mankin HJ, Dorfman H, Lippiello L, Zarins A. Biochemical and metabolic abnormalities in articular cartilage from osteo-arthritic human hips. II. Correlation of morphology with biochemical and metabolic data. J Bone Joint Surg Am 1971;53:523–37.
21. Mankin HJ. Biochemical and metabolic abnormalities in osteoarthritic human cartilage. Fed Proc 1973;32:1478–80.
22. Lee SW, Lee HJ, Chung WT, Choi SM, Rhyu SH, Kim DK, et al. TRAIL induces apoptosis of chondrocytes and influences the pathogenesis of experimentally induced rat osteoarthritis. Arthritis Rheum 2004;50:534–42.
23. Pettersen I, Figenschau Y, Olsen E, Bakkelund W, Smedsrod B, Sveinbjornsson B. Tumor necrosis factor-related apoptosis-inducing ligand induces apoptosis in human articular chondrocytes in vitro. Biochem Biophys Res Commun 2002;296:671–6.
24. Hayami T, Pickarski M, Zhuo Y, Wesolowski GA, Rodan GA, Duong LT. Characterization of articular cartilage and subchondral bone changes in the rat anterior cruciate ligament transection and meniscectomized models of osteoarthritis. Bone 2006;38:234–43.
25. Kong YY, Feige U, Sarosi I, Bolon B, Tafuri A, Morony S, et al. Activated T cells regulate bone loss and joint destruction in adjuvant arthritis through osteoprotegerin ligand. Nature 1999; 402:304–9.
26. Redlich K, Hayer S, Maier A, Dunstan CR, Tohidast-Akrad M, Lang S, et al. Tumor necrosis factor α-mediated joint destruction is inhibited by targeting osteoclasts with osteoprotegerin. Arthritis Rheum 2002;46:785–92.
27. Romas E, Sims NA, Hards DK, Lindsay M, Quinn JW, Ryan PF, et al. Osteoprotegerin reduces osteoclast numbers and prevents bone erosion in collagen-induced arthritis. Am J Pathol 2002;161: 1419–27.
28. Campagnuolo G, Bolon B, Feige U. Kinetics of bone protection by recombinant osteoprotegerin therapy in Lewis rats with adjuvant arthritis. Arthritis Rheum 2002;46:1926–36.
29. Emery JG, McDonnell P, Burke MB, Deen KC, Lyn S, Silverman C, et al. Osteoprotegerin is a receptor for the cytotoxic ligand TRAIL. J Biol Chem 1998;273:14363–7.
30. Wiley SR, Schooley K, Smolak PJ, Din WS, Huang CP, Nicholl JK, et al. Identification and characterization of a new member of the TNF family that induces apoptosis. Immunity 1995;3:673–82.
31. Schulze-Osthoff K, Ferrari D, Los M, Wesselborg S, Peter ME. Apoptosis signaling by death receptors. Eur J Biochem 1998;254: 439–59.
32. Pritzker LB, Scatena M, Giachelli CM. The role of osteoprotegerin and tumor necrosis factor-related apoptosis-inducing ligand in human microvascular endothelial cell survival. Mol Biol Cell 2004;15:2834–41.
33. Poole AR. An introduction to the pathophysiology of osteoarthritis. Front Biosci 1999;4:D662–70.
34. Santori N, Villar RN. Arthroscopic findings in the initial stages of hip osteoarthritis. Orthopedics 1999;22:405–9.
35. Pettit AR, Ji H, von Stechow D, Muller R, Goldring SR, Choi Y, et al. TRANCE/RANKL knockout mice are protected from bone erosion in a serum transfer model of arthritis. Am J Pathol 2001;159:1689–99.
36. Hayami T, Pickarski M, Wesolowski GA, Mclane J, Bone A, Destefano J, et al. The role of subchondral bone remodeling in osteoarthritis: reduction of cartilage degeneration and prevention of osteophyte formation by alendronate in the rat anterior cruciate ligament transection model. Arthritis Rheum 2004;50:1193–206.
37. Myers SL, Brandt KD, Burr DB, O'Connor BL, Albrecht M. Effects of a bisphosphonate on bone histomorphometry and dynamics in the canine cruciate deficiency model of osteoarthritis. J Rheumatol 1999;26:2645–53.

J Orthop Sci (2008) 13:173–179
DOI 10.1007/s00776-008-1213-y

JOURNAL OF
ORTHOPAEDIC SCIENCE

Original article

Japanese Orthopaedic Association Back Pain Evaluation Questionnaire. Part 3. Validity study and establishment of the measurement scale

Subcommittee on Low Back Pain and Cervical Myelopathy Evaluation of the Clinical Outcome Committee of the Japanese Orthopaedic Association, Japan

Mitsuru Fukui[1], Kazuhiro Chiba[2], Mamoru Kawakami[3], Shin-ichi Kikuchi[4], Shin-ichi Konno[4], Masabumi Miyamoto[5], Atsushi Seichi[6], Tadashi Shimamura[7], Osamu Shirado[8], Toshihiko Taguchi[9], Kazuhisa Takahashi[10], Katsushi Takeshita[6], Toshikazu Tani[11], Yoshiaki Toyama[3], Eiji Wada[12], Kazuo Yonenobu[13], Takashi Tanaka[14], and Yoshio Hirota[15]

[1] Laboratory of Statistics, Osaka City University Faculty of Medicine, Osaka, Japan
[2] Department of Orthopaedic Surgery, Keio University, Tokyo, Japan
[3] Department of Orthopaedic Surgery, Wakayama Medical University, Wakayama, Japan
[4] Department of Orthopaedic Surgery, School of Medicine, Fukushima Medical University, Fukushima, Japan
[5] Department of Orthopaedic Surgery, Nippon Medical School, 1-1-5 Sendagi, Bunkyo-ku, Tokyo 113-8603, Japan
[6] Department of Orthopaedic Surgery, The University of Tokyo, Tokyo, Japan
[7] Department of Orthopaedic Surgery, Iwate Medical University School of Medicine, Morioka, Japan
[8] Department of Orthopaedic Surgery, Saitama Medical School, Iruma-gun, Japan
[9] Department of Orthopaedic Surgery, Yamaguchi University School of Medicine, Yamaguchi, Japan
[10] Department of Orthopaedic Surgery, Graduate School of Medicine, Chiba University, Chiba, Japan
[11] Department of Orthopaedic Surgery, Kochi Medical School, Kochi, Japan
[12] Department of Orthopaedic Surgery, Hoshigaoka Koseinenkin Hospital, Osaka, Japan
[13] National Hospital Organization Osaka-Minami Medical Center, Kawachinagano, Japan
[14] Department of Internal Medicine, Houai Hospital, Osaka, Japan
[15] Department of Public Health, Osaka City University Faculty of Medicine, Osaka, Japan

Abstract

Background. The Japanese Orthopaedic Association decided to revise the JOA score for low back pain and to develop a new outcome measure. In February 2002, the first survey was performed with a preliminary questionnaire consisting of 60 evaluation items. Based on findings of that survey, 25 items were selected for a draft of the JOA Back Pain Evaluation Questionnaire (JOABPEQ). The second survey was performed to confirm the reliability of the draft questionnaire. This article further evaluates the validity of this questionnaire and establishes a measurement scale.

Methods. The subjects of this study consisted of 355 patients with low back disorders of any type (201 men, 154 women; mean age 50.7 years). Each patient was asked to fill in a self-administered questionnaire. Superficial validity was checked in terms of the completion rate for filling out the entire questionnaire. Factor analysis was then performed to evaluate the validity of the questionnaire and establish a measurement scale.

Results. As a result of the factor analysis, 25 items were categorized into five factors. The factors were named based on the commonality of the items: social function, mental health, lumbar function, walking ability, and low back pain. To establish a measurement scale for each factor, we determined the coefficient for each item so the difference between the maximum factor scores and minimum factor scores was approximately 100. We adjusted the formula so the maximum for each factor score was 100 and the minimum was 0.

Conclusions. We confirmed the validity of the JOA Back Pain Evaluation Questionnaire and est ablished a measurement scale.

Offprint requests to: M. Miyamoto
Received: September 25, 2007 / Accepted: January 10, 2008

Introduction

The evaluation criteria were based on physiological, biological, and anatomical outcome measure results of the Japanese Orthopaedic Association (JOA) score for low back pain.[1] The criteria include laboratory values, physiological findings, and imaging findings. These findings are significant for doctors but have little meaning for patients. From a patient's perspective, the presence of a symptom or its degree and functional condition

must have real meaning. This means that outcome measures need to be translatable from an objective evaluation to a subjective one, or from the doctor's perspective to the patient's perspective. The JOA decided to revise the JOA score for low back pain and develop a new scientific, patient-oriented outcome measure.

The first committee meeting was held in June 2000, and the first survey was initiated in February 2002 using a preliminary questionnaire consisting of 60 items. It was a self-administered, disease-specific measure developed with reference to the Japanese editions of SF-36[2,3] and the Roland-Morris Disability Questionnaire (RDQ)[4,5] to assess health-related quality of life. Based on findings of the survey, 25 items were selected for a draft of the JOA Back Pain Evaluation Questionnaire (JOABPEQ) (see Appendix 1).

The second survey was started in January 2004 to evaluate the reliability of the 25 items selected for the draft JOABPEQ. We successfully confirmed the reliability, and these details have been described in previous reports of Part 1[6] and Part 2.[7] Part 3 of this study involves further development of the new JOA questionnaire, evaluation of the validity of the draft JOABPEQ, and establishment of a measurement scale.

Materials and methods

Recruitment of patients

A total of 369 of the 829 Japanese board-certified spine surgeons were randomly selected and asked to recruit at least three patients each to participate in evaluating the JOABPEQ during February 2004. The inclusion criterion was any type of lumbar spine disorder. Exclusion criteria were patients who had:

- Other musculoskeletal diseases requiring medical treatment
- Psychiatric disease, potentially leading to inappropriate answers
- Postoperative condition
- Participation in previous surveys related to this study

Testing the questionnaire

Each patient was asked to fill in the self-administered questionnaire. The attending surgeon filled out information on the diagnosis, presence or absence of concomitant diseases, and a judgment regarding the severity of symptoms using a three-step rating scale (mild, moderate, severe). The severity of the symptoms was determined subjectively by the attending surgeon, who was asked not to select a similar patient based only on the severity. This study was approved by the Ethics Committee of the Japanese Society for Spine Surgery and Related Research, and informed consent was obtained from each patient.

Factor analysis was used to check the statistical validity of the questionnaire and establish the measurement scale. All statistics were calculated using SPSS software (version 12; SPSS, Chicago, IL, USA).

Results

Patient characteristics

Of the 452 patients selected for participation in this survey, 1 patient who was judged inappropriate by the attending doctor and 60 patients with other musculoskeletal diseases requiring medical treatment were excluded. The responses from 36 patients who answered incompletely were also excluded, leaving 355 patients available for analysis: 201 men and 154 women, with a mean ± SD age of 50.7 ± 18.0 (Table 1). The diagnosis was lumbar disc herniation in 167, lumbar spinal canal stenosis in 103, and spondylolisthesis in 37.

According to the judgment of the attending doctor, there were 115 mild, 142 moderate, and 98 severe cases. Table 2 summarizes the severity of low back pain evaluated by the current JOA scoring system and shows that the characteristics of the recruited patients were not

Table 1. Distribution of age and severity of symptoms ($n = 355$)

	Severity of symptoms			
Age (years)	Mild	Moderate	Severe	Total
Males				
10–19	3	4		7
20–29	8	4	9	21
30–39	12	14	6	32
40–49	12	14	8	34
50–59	12	9	11	32
60–69	10	12	12	34
70–79	11	16	8	35
80+	4	2		6
Total	72	75	54	201
Females				
10–19	0	1	3	4
20–29	9	5	5	19
30–39	7	13	10	30
40–49	5	14	7	26
50–59	4	9	5	18
60–69	7	12	7	26
70–79	11	10	4	25
80+		3	3	6
Total	43	67	44	154
Total no.	115	142	98	355